Annalisa Martorana, **Martina Lenzuni**, Marco Contardi, Fabio S. Palumbo, Salvatore Cataldo, Alberto Pettignano, Valentina Catania, Domenico Schillaci, Maria Summa, Athanassia Athanassiou, Calogero Fiorica, Rosalia Bertorelli, and Giovanna Pitarresi

Schiff Base-Based Hydrogel Embedded with *In Situ* Generated Silver Nanoparticles Capped by a Hyaluronic Acid–Diethylenetriamine Derivative for Wound Healing Application

ACS Applied Materials & Interfaces **2024** *16* (16), 20186-20201

The final published version (version of record) is available online via ACS Publications at: https://doi.org/10.1021/acsami.4c00657

Publisher:

American Chemical Society

Date:

Apr 1, 2024

Schiff Base-based Hydrogel Embedded with In-situ Generated Silver Nanoparticles Capped by a Hyaluronic Acid-diethylenetriamine Derivative for Wound Healing Application

Annalisa Martorana[1], Martina Lenzuni[2,†,], Marco Contardi[2,*], Fabio S. Palumbo[1,*], Salvatore Cataldo[3], Alberto Pettignano[3], Valentina Catania[4], Domenico Schillaci[1], Maria Summa[5], Athanassia Athanassiou[2], Calogero Fiorica[1], Rosalia Bertorelli[5,§], Giovanna Pitarresi[1,§]*

[1] Department of Biological, Chemical, and Pharmaceutical Sciences and Technologies (STEBICEF), University of Palermo, Via Archirafi 32, 90123, Palermo, Italy

[2] Smart Materials, Istituto Italiano di Tecnologia, Via Morego 30, 16163, Genova, Italy

[3] Department of Physics and Chemistry – Emilio Segrè, University of Palermo, Viale delle scienze, Ed. 17, 90128, Palermo, Italy

[4] Department of Earth and Marine Sciences (DiSTeM), University of Palermo, Viale delle Scienze Ed. 16, 90128, Palermo, Italy

[5] Translational Pharmacology, Istituto Italiano di Tecnologia, Via Morego 30, 16163, Genova, Italy

KEYWORDS: Schiff Base, dynamic covalent linkage, self-healing, pH-responsive linkage, silver nanoparticles, antibacterial hydrogel

ABSTRACT

In this study, hydrogels were produced using a Schiff base reaction between two hyaluronic acid derivatives, one containing aldehyde groups (HA-Ald) and the other holding a diethylene triamine with terminal amino groups (HA-DETA). The DETA portion promote the in-situ growth, complexation, and stabilization of silver nanoparticles (AgNPs), eliminating the need for external reducing agents. The reaction between HA-DETA and HA-Ald leads to the formation of imine bonds, which results in dynamically pH-responsive crosslinking. While DETA capping ability helped in embedding the AgNPs, the on/off pH environmental responsivity of the hydrogel allows for a controlled and on-demand release of the drugs, mainly

when bacterial infections cause pH variation of the wound bed. The injectable hydrogels resulted in being highly compatible in contact with blood red cells, fibroblasts, and keratinocytes, and capable of having a proliferative effect on an in vitro wound scratch model. The pH-responsive hydrogels showed proper antibacterial activity against Pseudomonas aeruginosa and Staphylococcus aureus, common bacterial strains presented in wound infections. Finally, in vivo wound model studies demonstrated an overall speeding up in the wound healing rate and an advanced wound condition in the experimental group treated with the hydrogels compared to control samples.

1. INTRODUCTION

Injectable hydrogels are promising in tissue engineering (TE), offering an alternative to costly surgical implants and improving patient compliance.[1–4] Traditional natural hydrogels with non-reversible covalent linkages can be damaged during injection due to pressure from delivery devices and, additionally, they can be reabsorbed too quickly with limited utility due to suboptimal mechanical properties.[5–7] While these limitations can be mitigated through in-situ gelation at the target site using ionotropic crosslinked polymers,[8–10] damage can still occur post-injection due to mechanical forces resulting from bodily movements.[11] This failure of the

hydrogels can lead to rapid degradation and leakage of loaded drugs resulting in unsatisfactory therapy.[12–14] On the other hand, permanently crosslinked hydrogels are unsuitable for cell delivery, as they could hinder cell growth, [15–18] and struggle to adapt and maintain continuous contact with irregular injury sites fully.[19,20] Therefore, their use at the clinical level utility is still limited.

By contrast, polymeric networks with dynamic covalent chemistry based on reversible interactions can offer superior performance in injectability, mechanical properties, and self-healing capacity that are often desirable across various biomedical applications.[21–26]

In the covalent linkages used to prepare self-healing hydrogels, the imine bond emerges through the reversible Schiff base reaction between an aldehyde/ketone and an amino group. This click chemistry reaction occurs swiftly under physiological conditions, exhibiting high chemical selectivity.[20,27,28] Consequently, when the network structure faces disruption, these linkages promptly re-engage, restoring the original hydrogel matrix. Biomaterials endowed with these properties can rapidly undergo self-repair following injection, offering mechanical support or safeguarding loaded cells.[29] Furthermore, these hydrogels can comprehensively cover and effectively fill non-uniform injured sites, withstanding mechanical forces resulting from bodily movements or organ activities. This makes them highly efficient in the context of

wound healing.[20,30] Additional advantages associated with using Schiff base bonds include their smart and reversible pH responsiveness. This property opens up the potential for these hydrogels to serve as carriers for drugs in wound and cancer treatment, facilitating the controlled release of therapeutic agents to meet specific treatment requirements.[31,32] In particular, severely infected wounds are characterized by a changing of the pH in the wound bed due to the byproducts of the bacterial metabolic activity. This severe and progressive infection can develop phenomena of antibiotic resistance in time, making using antibacterial substances that do not induce antimicrobial resistance, such as silver nanoparticles, increasingly important.[33] During the initial stages of bacterial infection, wounds become locally acidified, and pH-responsive hydrogels can produce an on-demand action, help minimize side effects, and improve the potential for more effective treatment.[34,35] Silver nanoparticles (AgNPs), well-known for their potent antibacterial properties,[20,36] have been also shown to stimulate anti-inflammatory responses, and facilitate the various stages of the healing process.[37,38] The use of self-healing hydrogels loaded with antibacterial AgNPs proves to be advantageous to mitigate the toxicity concern, and to enable sustained drug delivery,[39–42] acting as reservoirs for drugs and facilitating localized release at the target site. This approach reduces side effects and circumvents the challenges associated with systemic administration.[39]

This work aims to develop a self-healing hydrogel based on hyaluronic acid, which serves as injectable biomaterial and antibacterial platform for the controlled and pH-responsive release of silver nanoparticles (AgNPs) for wound treatment. Hyaluronic acid (HA) is a critical component of the extracellular matrix (ECM) with a pivotal role in various biological processes like cell growth, differentiation, signaling, matrix organization, and wound repair.[43–45] By chemical derivatization of HA dynamically crosslinked hydrogels can be obtained for wound healing purposes. Here, aldehyde groups were introduced by oxidizing HA with $NaIO_4$ and simultaneously, an amino HA derivative was obtained, as described in our previous work, utilizing diethylene triamine (DETA).[46] In particular, DETA segments served as capping ions, facilitating the in-situ synthesis of nano-sized AgNPs under mild, reducing agent-free conditions. These modified hyaluronic acid derivatives can undergo a one pot click chemistry reaction, forming self-healing hydrogels that act as reservoirs for AgNPs. The network formation involves both chemical and physical crosslinking mechanisms. Specifically, the protonation of the primary and secondary amino groups of HA-DETA contributes to additional physical interactions that reinforce the HA feature of a dual-crosslinked network.[46] Our study comprehensively examined various properties and characteristics of these hydrogels, including gelling time, morphology, swelling ratio, degradation, rheology and self-healing capability.

Additionally, in vitro biocompatibility, hemolysis rates, and antibacterial tests against Gram-negative and Gram-positive pathogens commonly associated with chronic wounds were assessed. Finally, the capacity of the hydrogels to speed up the rate and the condition of an injury was tested in a mouse model. These assessments provide valuable insights into the potential of these hydrogels for combating wound infections and promoting effective wound healing.

2. RESULTS AND DISCUSSION

2.1 Hydrogels preparation and characterization

In our previous study, the HA-DETA derivative underwent extensive characterization.[46] The synthesis and characterization of the HA-aldehyde derivative (HA-Ald) followed the procedure outlined in the literature by Su et al., and it is reported in Supplementary data section S1 and Figure S1a, S1b and S1c.[47–49]

Figure 1a and 1b depict a schematic representation of the hydrogel preparation procedure. Specifically, for the production of AgNPs-based hydrogels, a dispersion of AgNPs/HA-DETA was first prepared. The diethylenetriamine (DETA) portion contains N donor atoms capable of coordinating Ag^+ ions and promoting controlled growth of the nanoparticles.[50] This enhances

HA's efficiency in reducing silver ions and stabilizing AgNPs, thereby preventing nanoparticle aggregation. Furthermore, Ag nanoparticles capped with HA-DETA help overcome toxicity, minimizing cytotoxicity and environmental impact.[46,51]

For hydrogel production, HA-Ald was introduced into the HA-DETA or HA-DETA/AgNPs dispersion with continuous mixing, leading to the immediate formation of the hydrogel. By tuning the volumetric ratio between HA-Ald and HA-DETA or HA-DETA/AgNPs, a broad range of molar ratios between aldehyde (CHO) and amino (NH_2) groups was achieved, spanning from 0.3 to 1.77, named $F_{1.77}$, $F_{1.14}$, $F_{0.89}$ and $F_{0.30}$ and $AgF_{1.77}$, $AgF_{1.14}$, $AgF_{0.89}$ and $AgF_{0.30}$, where F stands for the molar "feed ratio" followed by a number which indicate the molar ratio CHO/NH_2, as illustrated in Table S1. Crosslinking was achieved through the reaction between HA-DETA and HA-Ald, resulting in the formation of imine bonds.

For the samples $F_{0.30}$, $F_{0.89}$, $F_{1.14}$, and $F_{1.77}$ hydrogels, the degree of crosslinking was found to be 62%, 85%, 88%, and 93%, respectively. This increase in crosslinking efficiency corresponds to the increasing molar ratio CHO/NH_2. To confirm the chemical structure of the hydrogels, fourier-transform infrared spectroscopy (FT-IR) was employed (Figure S2a).

Moreover, scanning electron microscope (SEM) observed AgNPs loaded hydrogels, confirming a uniform and homogeneous distribution of nanoparticles into the matrix (Figure S2b).

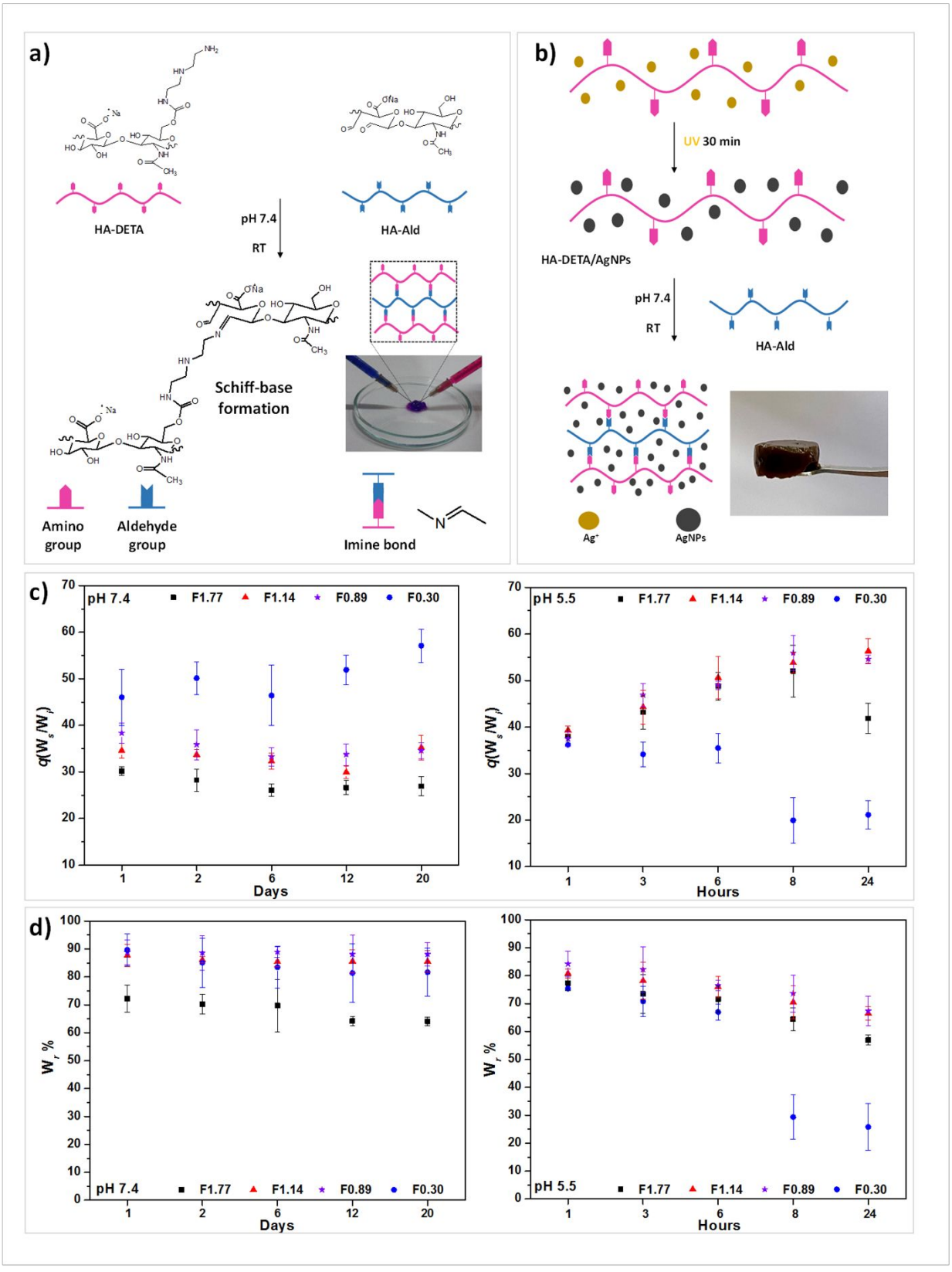

Figure 1. Schematic representation of hydrogel production without (polymer dispersions were previously stained with Rhodamine B and Azure II) (a) and with (b) AgNPs with inserts

showing photographs of the hydrogels; Bar graphs of swelling (c) and degradation (d) results of the hydrogels kept in phosphate buffer pH 5.5 and pH 7.4.

The gelation time is a critical factor in designing in-situ forming hydrogels; if the gelation time is too long, the polymer dispersions can undergo leaching after injection. Rapid gelling is a required property of an injectable hydrogel to quickly fill the entire defect surface.[52] Therefore, achieving an appropriate gelation time is essential for enabling the application of the resulting hydrogel through in-situ injection. It was observed that all the hydrogels exhibited a gelation time of less than 25 seconds, and the levels of aldehyde and amino groups significantly influenced this time. As the CHO/NH_2 ratio increased, the gelation time decreased. This is attributed to the higher number of reactive sites available for forming Schiff bases, leading to more efficient crosslinking (see Table S1). These findings align with those reported by Qu et al., who concluded that increasing the CHO/NH_2 molar ratios accelerates the gelation of Schiff base-based hydrogels.[53] Specifically, the gelation times for $F_{1.77}$, $F_{1.14}$, $F_{0.89}$, and $F_{0.30}$ were approximately 8, 12, 19, and 22 seconds, respectively, as summarized in Table S1.

Figure 1c illustrates how the swelling, expressed as q value, at physiological pH, increases as the molar ratio CHO/NH_2 decreases for all the analyzed time points (from 1 to 20 days of

analysis), by a lower crosslinking efficiency. Samples $F_{1.77}$, $F_{1.14}$, and $F_{0.89}$ showed an almost constant value of swelling over time, suggesting prolonged (up to 20 days) resistance of hydrogels at physiological pH. Notably, the less crosslinked hydrogel ($F_{0.30}$) exhibited a q value almost double that of $F_{1.77}$ throughout the analysis (p <0.01).

At pH 5.5, $F_{1.77}$, $F_{1.14}$, and $F_{0.89}$ exhibited a sharp increase in the swelling rate compared to the behavior at physiological pH, even within 8 hours (the analysis in this case was performed within 24 hours), suggesting very pronounced pH responsiveness of hydrogels. This prompt pH-responsive behavior could be attributed, on the one hand, to the known effect of an acidic environment, which promotes amine protonation, leading to the breakage of Schiff base bonds and enhancing the pore connectivity of the hydrogel, allowing it to retain more water.[24] On the other hand, the pH responsiveness of the HA-DETA derivative itself plays a role. As described in our previous work, the secondary amino group of DETA allows for partial protonation at acidic pH, which could increase inter-chain repulsion and thus enhance pH-responsive hydrogel swelling. In contrast, less crosslinked hydrogels $F_{0.30}$ showed an initial gradual decrease in swelling followed by a significant drop at 8 and 24 hours due to the dissolution of the hydrogel within the 8 hours (Figure 1c).

The degradation data at pH 7.4 reveal that the weight recovered at the specified times throughout the 20 days of analysis decreases as the molar ratio CHO/NH_2 increases, and thus, the crosslinking efficiency increases (Figure 1d). The $F_{1.77}$ sample shows a much higher degradation with a loss weight of 30-20% (p <0.01). This seemingly contradictory result can be explained by considering that samples with higher crosslinking efficiency are produced using a more significant amount of HA-Ald, which, due to its lower molecular weight, can be easily washed out and diffusing from the hydrogel, thus reducing the actual weight of the hydrogel recovered. In the acidic pH, coherently with swelling data, very sharp pH responsiveness was noticed, with the rate of hydrolysis increasing significantly within 24 hours. At this pH, according to the better crosslinking efficiency, samples $F_{1.77}$, $F_{1.14}$, and $F_{0.89}$ showed enhanced stability compared to the $F_{0.30}$ sample, which was almost completely dissolved within 24 hours.

No statistically significant difference was observed in the presence and absence of AgNPs, demonstrating that the latter do not influence the behavior of the hydrogels in swelling and degradation studies.

2.2 Rheological studies and self-healing experiments

Rheological viscosity-shear rate flow sweep measurements indicated that these hydrogels exhibit shear-thinning behavior. The data presented in Figure 2a illustrate a decrease in viscosity for all different molar ratios hydrogels as the shear rate increased from 0.01 to 100 s^{-1}, ranging from 10^4 – 10^5 Pa·s at 0.01 s^{-1} to 1-15 Pa·s at 100 s^{-1}. This behavior allows for injection through a needle under shear stress, with subsequent recovery once the shear stress is removed.[54,55] This behavior made gel injection through a 20G needle feasible for all samples (Figure 2a). The impact of the molar ratio on the mechanical properties of these hydrogels was investigated through rheological strain and frequency sweep experiments (Figure 2b and 2c). Figure 2b depicts that the storage modulus (G') is greater than and parallel to the viscous modulus (G") at low strain values. Both moduli decrease at high strain values exceeding 80%, marking the onset of the non linear viscoelastic region. There's a crossover point at a critical strain value within the range of 150-200%, at which the value of G' sharply declines, falling below that of G", indicating network destruction within the hydrogel. The linearity zone is delimited at high strain percentages by the deviation from the linear behavior of the elastic modulus. Specifically, as the molar ratio CHO/NH_2 increases, both G' and G" increase while the extent of the linearity zone decreases. Higher values of the elastic modulus suggest greater hydrogel rigidity and, consequently, lower critical strain percentages at which polymer network

breakdown occurs, narrowing the LVR. These results align with the degree of crosslinking within the hydrogels dictated by the CHO/NH_2 molar ratio.

As shown in Figure 2c, the G' modulus exhibited a slight increase for all samples. It consistently remained higher than the G" modulus across the entire analyzed frequency range, indicating an elastic behavior and a gel-like state of the samples. While G' remained relatively stable, signifying consistent network formation, G" displayed some frequency fluctuations. A similar trend was recorded by Wang et al. and Mondal et al. in their self-healing double network systems.[52,56] The viscous modulus showed a minimum at an angular frequency that decreased as the CHO/NH_2 molar ratio decreased. As the angular frequency increased, the ratio between G' and G" also increased, forming a more stable structure, a characteristic behavior of Schiff bases attributed to the presence of dynamic and reversible bonds.

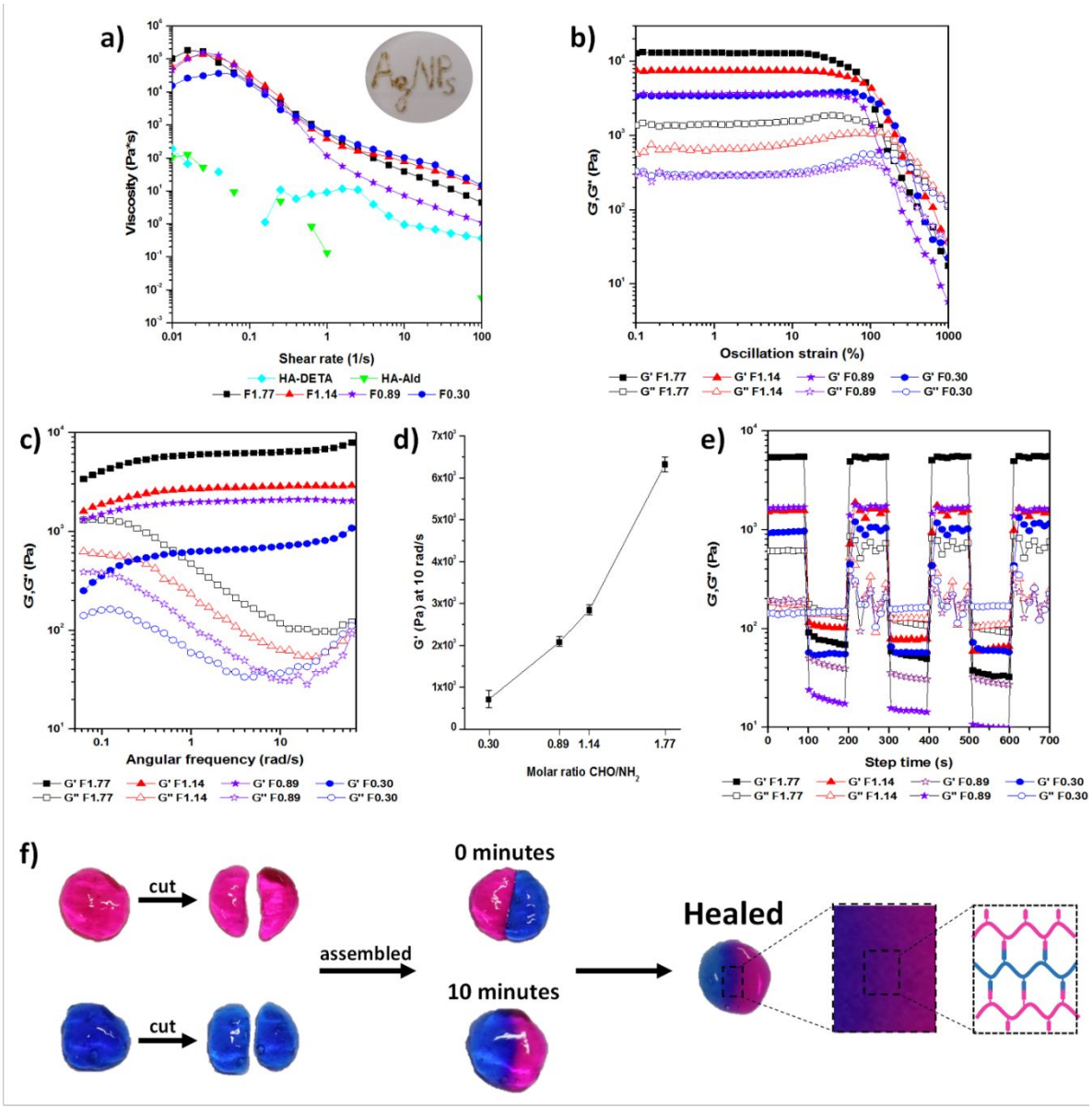

Figure 2. Flow (a), Strain, (b) Frequency (c) sweep analysis of samples $F_{1.77}$, $F_{1.14}$, $F_{0.89}$, and $F_{0.30}$; relation between elastic modulus G′ (at 10 rad/s) and molar ratio (d); step time recovery test of samples (e), self-healing experiments of hydrogels (f).

Additionally, as illustrated in Figure 2d, the G' modulus of the hydrogel increases with the CHO/NH_2 molar ratio, reaching, at 10 rad/s, values of approximately 700 Pa, 2.0 kPa, 2.8 kPa,

and 6.3 kPa for $F_{0.30}$, $F_{0.89}$, $F_{1.14}$, and $F_{1.77}$, respectively. This increase in G' with a higher CHO/NH_2 molar ratio results from forming of more imine bonds through the Schiff base reaction, attributed to a more significant number of aldehyde groups available for interaction with the amino groups of HA-DETA. This finding is consistent with increased crosslinking efficiency, as depicted in Table S1. A similar trend was observed by Qu et al., who analyzed the influence of different molar ratios on the mechanical properties of Schiff base-based hydrogels made of N-carboxyethyl chitosan (CEC) and dibenzaldehyde-terminated poly(ethylene glycol) (PEGDA) showing G′ values ranging from 8 to 25 kPa.[53,57]

Recovery time studies were also conducted to monitor the self-healing ability, as depicted in Figure 2e. For all CHO/NH_2 ratios tested, the G' value significantly drops under high strain due to damage to the hydrogel network. However, the G' storage modulus quickly and fully recovers as applied deformation decreases, demonstrating the excellent self-healing capability of the hydrogels after damage. Specifically, there is nearly instant recovery for all hydrogels, with G' and G'' moduli switching places when subjected to high strain. Additionally, a noteworthy observation is the decrease in the elastic modulus during deformation cycles, with values dropping by two orders of magnitude when subjected to high strain percentages.

Macroscopic evaluations of self-healing ability involved placing two equal gel pieces, prepared in different colors, together in an alternating color pattern at 25 ˚C.[58,59] Approximately 10-30 minutes later, these gel slices formed a complete hydrogel disc, showcasing the dynamic reactions between the two functional groups (Figure 2f). After disruption and self-healing, the hydrogels completely regained their elastic properties, as demonstrated by comparing the G' modulus measured on hydrogels previously disrupted using a mortar and pestle (Figure S3a and b).

The bar graph in Figure S3b illustrates no statistically significant differences between freshly prepared and healed hydrogels, affirming the complete repair of the hydrogels. These properties can offer a solution in case of damages from the intense pressure applied by injection devices or mechanical forces resulting from body movement by autonomously repairing structural defects and restoring functionality, promoting stability post-administration.[60]

Notably, the $F_{0.30}$ hydrogel exhibited a "self-repair" process within 10 minutes (Figure 2f and S3c). The hydrogel's self-healing abilities stem from dynamic bonds, continuously breaking and self-repairing. Furthermore, due to the polyampholyte nature of the HA-DETA derivative, it is conceivable that interactions between the COOH glucuronic groups and the amino portions

of the DETA introduced into the polymer backbone of HA contribute to hydrogel entanglement.

The intensity of these interactions, as discussed in the previous paragraph, is closely linked to the environmental pH, remaining stable at neutrality while cooperating with dynamic Schiff base bonds and rapidly dissolving at acidic pH due to the protonation of DETA amino groups and consequent repulsion. Both chemical and physical bonds contributed to a relatively high self-healing ability.

No statistically significant difference was observed in the presence and absence of AgNPs for all the studies conducted.

2.3 pH responsiveness and silver release

Figure 3a presents the samples' elastic modulus (G′) after being immersed in phosphate buffers at pH 5.5 or 7.4 for 24 hours. The elastic modulus experiences a substantial decrease, reaching values of significantly lower magnitude for samples maintained at pH 5.5 (Figure 3b). This analysis reaffirms the pronounced pH responsiveness of these hydrogels. To visually demonstrate the pH sensitivity of these hydrogels, hydrogel $F_{0.89}$ was selected. As depicted in

Figure S3d, adding of 1M HCl induces a transition from gel to sol, and subsequently, with the addition of 1M NaOH, a sol to gel transition occurs.

The results of the Ag^+ release study revealed a prolonged release of Ag^+ at nearly neutral pH conditions (Figure 3c), with a release rate that aligns with the hydrogel's crosslinking efficiency. Hydrogels $AgF_{1.77}$, $AgF_{1.44}$, and $AgF_{0.89}$ exhibited an initial release of 4% of Ag^+ during the first 2 days, after which Ag^+ diffusion ceased. In contrast, $AgF_{0.30}$ displayed a gradual and sustained release throughout the 20-day analysis period, with 27% of Ag^+ released. Conversely, at pH 5.5 (Figure 3d), a substantial release (70%) was observed after 3 hours for the hydrogel with a CHO/NH_2 molar ratio of 0.30, primarily due to the rapid dissolution of the hydrogel. The more crosslinked hydrogels exhibited an extended-release for up to 24 hours in response to the reduction in environmental pH. The robust capping ability of DETA segments allows for the tight retention of Ag^+ within the dynamically crosslinked hydrogel, making it highly susceptible to decreased pH levels, reversibly triggering network disassembly and immediate Ag^+ release.

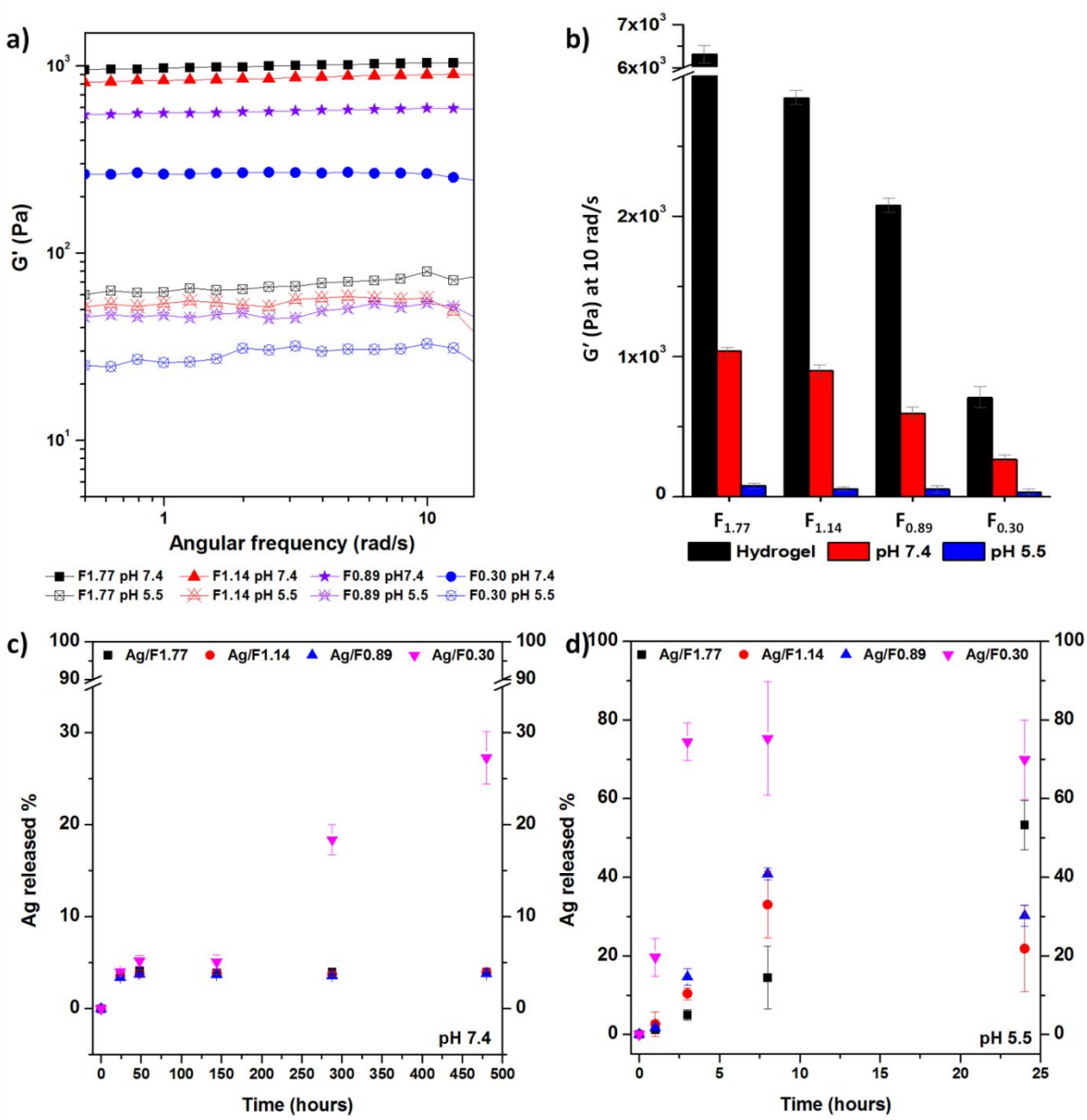

Figure 3. Frequency sweep analysis of samples previously kept in phosphate buffer at pH 7.4 or 5.5 for 24 hours (a); Bar graph of elastic modulus G′ (at 10 rad/s) of freshly prepared hydrogels and hydrogels kept in phosphate buffer at pH 7.4 or 5.5 (b); Release study of AgNPs loaded hydrogels in phosphate buffer at pH 7.4 (c) and pH 5.5 (d).

2.4 Antimicrobial studies

The preliminary evaluation of the antibacterial activity of AgNP-based hydrogels against reference strains *Pseudomonas aeruginosa* ATCC 15442 and *Staphylococcus aureus* ATCC 25923 was conducted based on the diameter of the zone of inhibition of free-living bacterial growth (see Figure 4a-b). The diffusion tests on agar against *P. aeruginosa* and *S. aureus* revealed the presence of an halo inhibition zone in all hydrogel samples, confirming their antibacterial properties. Hydrogels without nanoparticles did not exhibit any inhibition halos. Figure 4c-d presents the antibacterial activity of AgNP-based hydrogels in a liquid environment. All samples of AgNP-based hydrogels demonstrated substantial antimicrobial activity against both planktonic bacterial strains cultured in a Tryptic Soy Broth (TSB) medium at pH 5.5. However, no antimicrobial activity was observed against bacterial strains grown at pH 7.4, underscoring the influence of pH on the release of nanoparticles by the hydrogels. The presence of Ag nanoparticles combined with the pH reduction significantly decreased ($p < 0.001$) bacterial viability to approximately 4.08 x 10^6 CFU/mL (hydrogel $AgF_{0.30}$) and 1.02 x 10^7, 1.97 x 10^7, 2.6 x 10^7 CFU/mL (hydrogel $AgF_{1.77}$, $AgF_{1.14}$ and $AgF_{0.89}$ respectively) for *P. aeruginosa* (as shown in Figure 4c). The hydrogel $F_{0.30}$ exhibited a more remarkable ability to reduce bacterial counts compared to hydrogels with other molar ratios due to its rapid dissolution, especially than more crosslinked hydrogels. A logarithmic reduction of 2.8, 2.6,

2.5, and 3.2 was observed for hydrogels $AgF_{1.77}$, $AgF_{1.14}$, $AgF_{0.89}$, and $AgF_{0.30}$, respectively, compared to bacterial growth control without hydrogel.

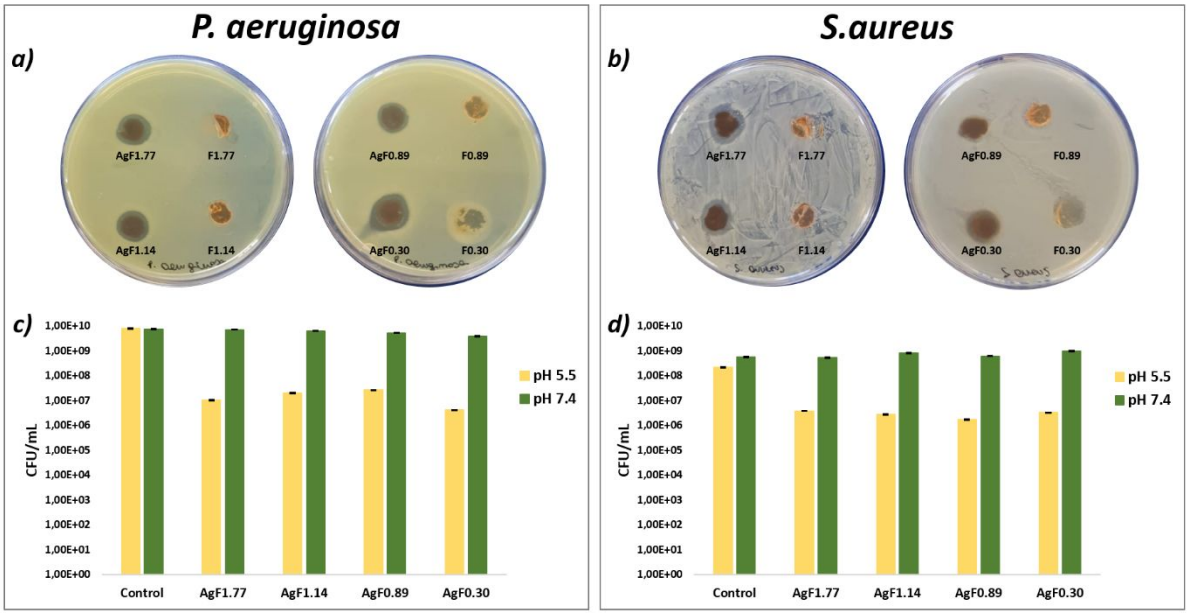

Figure 4. Inhibition zone diameter of $AgF_{1.77}$, $AgF_{1.14}$, $AgF_{0.89}$, and $AgF_{0.30}$ (samples on the left of each plate) or hydrogel without AgNPs (samples on the right of each dish) against *P. aeruginosa* ATTC 15442 (a) and *S.aureus* ATTC 25923 (b); Antibacterial activity against *P. aeruginosa* ATTC 15442 (c) and *S. aureus* ATCC 25923 (d) of $AgF_{1.77}$, $AgF_{1.14}$, $AgF_{0.89}$, and $AgF_{0.30}$. Histograms show the colony forming units (CFU/mL) of bacterial strains obtained by viable plate counts method after 24 hours of incubation.

In the case of *S. aureus* (Figure 4d), AgNP-based hydrogels, combined with pH 5.5, reduced ($p < 0.001$) the viable bacterial count to approximately 1.7 x 10^6 CFU/mL (hydrogel $AgF_{0.89}$), and 3.8 x 10^6, 2.74 x 10^6, 3.2 x 10^6 CFU/mL (hydrogel $AgF_{1.77}$, $AgF_{1.14}$ and $AgF_{0.30}$

respectively) resulting in a logarithmic reduction of 1.7, 1.9, 2.1 and 1.8 for hydrogels $AgF_{1.77}$, $AgF_{1.14}$, $AgF_{0.89}$, and $AgF_{0.30}$, respectively, compared to bacterial growth control without hydrogel. No significant differences in the viable bacterial strain *S. aureus* were observed among AgNP-based hydrogels with different molar ratios.

The results obtained against *P. aeruginosa* and *S. aureus* hold particular significance, as these two bacterial species frequently coexist in chronically infected wounds. Bacterial colonization of chronic wounds is closely linked to biofilm formation, leading to local and systemic inflammation.[61,62] This, in turn, imparts heightened resistance to host defenses and therapeutic treatments, ultimately exerting a detrimental impact on the healing process.

2.5 Cytocompatibility, wound scratch, and Hemocompatibility with mouse whole blood evaluation

In vitro cytocompatibility studies of hydrogels were performed on human fibroblast cells (NHDF) for 24 h and 48 h.

Figure S4a shows that no signs of toxicity were detected for all hydrogels with or without AgNPs, and no statistically difference was recorded. The observed optimal cellular viability for AgNPs-based hydrogels can be attributed to HA-DETA's ability to stabilize nanoparticles

and control the release of Ag^+, also confirmed by the Live and Dead assay (Figure 5a and S4b, c, d, and e).

The cytocompatibility was further tested on loaded NHDF into hydrogels without AgNPs. The fluorescent images showed that the encapsulated cells in the hydrogels are alive regardless of the degree of crosslinking present in the function of the different molar ratios of the tested samples (Figure S5).

Considering the remarkable ability to reduce bacterial counts by $F_{0.30}$ hydrogel this sample was further *in vitro* characterized before to be then tested in efficacy models. The cytocompatibility of $F_{0.30}$ hydrogel with and without AgNPs at different concentrations was also tested using keratinocytes (HaCaT cells) for 24 h and 48 h. The results are reported in Figure 5b and c, and no signs of toxicity were detected. Indeed, according to ISO10993-5 guidelines, a reduction of cell survival by less than 30% indicates no toxicity, and for all the tested concentrations, the viability resulted in being above this threshold. No statistically significant differences ($p > 0.05$) were observed in the cell survival compared to the control, confirming the excellent biocompatibility of these materials.

HaCaT cells were used for the wound scratch test. After the wound induction, HaCaT were observed for 48 hours to assess the effect on the wound closure rate. The distance between the

edges of the wound monolayer was measured using ImageJ software as the mean distance. Images of the different conditions at 0, 24, and 48 h are shown (Figure 5d). Keratinocytes treated with $F_{0.30}$ and $AgF_{0.30}$ materials could heal the wound scratch faster with respect to the untreated sample. Specifically, after 24 h, the wound closure in the control samples was less than 20%, whereas it had already reached 35–49% in the presence of the $F_{0.30}$ and $AgF_{0.30}$ samples (Figure 5e). At 48 h, the wound was almost closed in the presence of $F_{0.30}$ and $AgF_{0.30}$ (62–85%), while CTRL was less than 55%. These results suggest the ability of these materials to increase the keratinocytes' proliferation.

The initial stage of wound healing that takes place right after an injury is known as hemostasis. It is defined by the first clotting process that occurs to aid in bleeding management. Diabetes frequently interferes with hemostasis and prolongs the first phase of wound healing due to the abnormality of hemostatic system components.[63,64]

To be considered suitable for tissue regeneration, the hydrogels should present a hemolysis value of less than 5%, a limit set by the ISO 10993-4 standard. Notably, all the tested hydrogels ($F_{0.30}$ and $AgF_{0.30}$) showed a low hemolysis rate (HR) with mice erythrocytes (Figure 5f). In particular, $F_{0.30}$ hydrogels exhibited a negligible hemolysis ratio (0.19% and 0.56% for the 100 and 200 μL hydrogels, respectively). When AgNPs were added to the hydrogels, the hemolysis

rates showed a significant increase only in the case of the 200 μL $AgF_{0.30}$ hydrogels (HR = 4.1%) and not in the case of the 100 μL $AgF_{0.30}$ hydrogels (HR = 2.3%). The hemolysis percentage of all tested hydrogels was lower than 5%, reflecting good hemocompatibility. The obtained data are also in accordance with published literature regarding hemolysis rates on hyaluronic-based hydrogels.[65–68] Moreover, our results agree with previous studies that demonstrated the pro-hemolytic properties of AgNPs, even if the mechanism of this induced hemolysis has not yet been completely elucidated.[69–71]

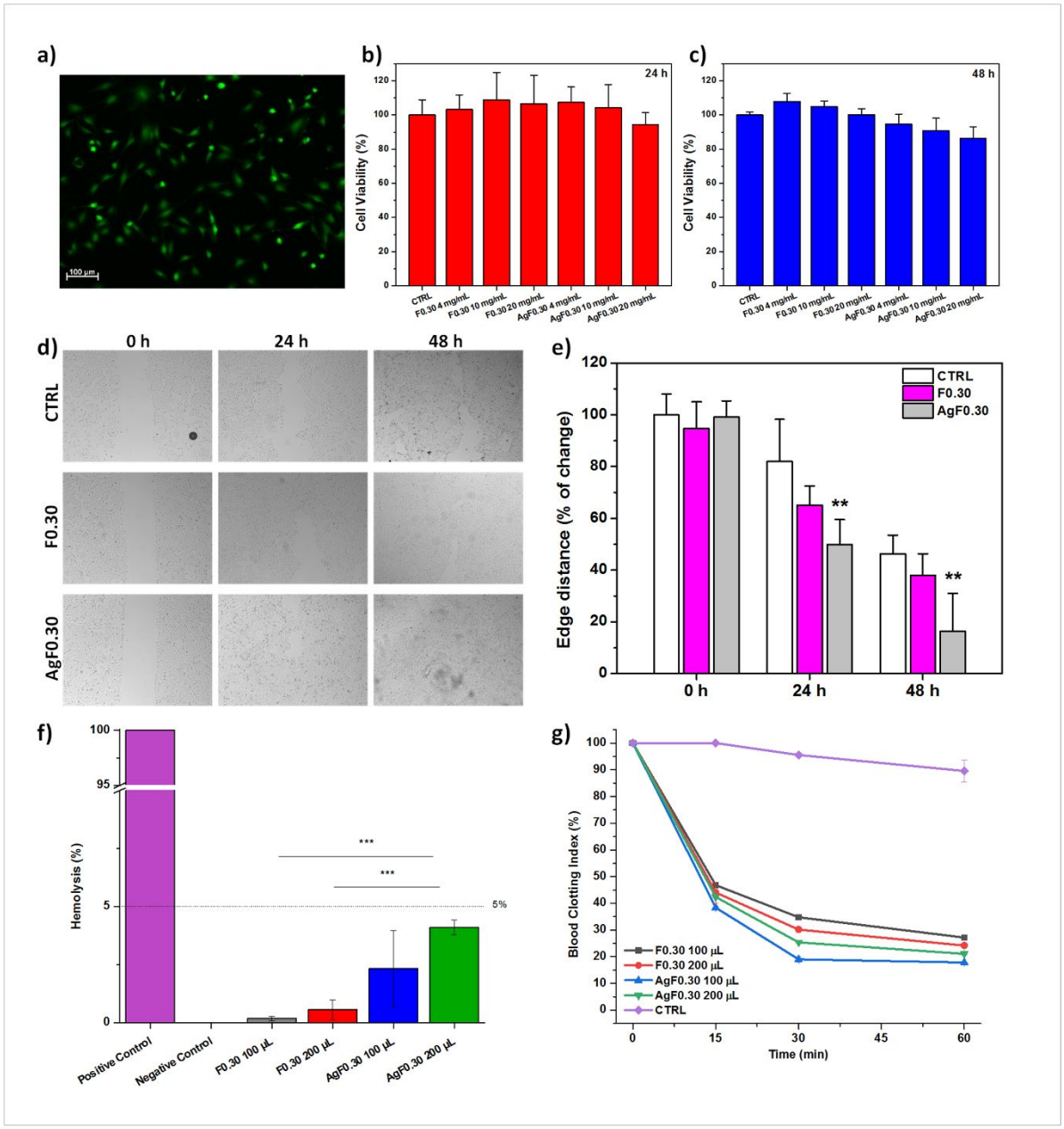

Figure 5. Fluorescent image of NHDF incubated with hydrogel $AgF_{0.30}$ for 48 h (a); Histogram of cell viability of HaCaT cells incubated for 24 h (b) and 48 h (c) with 4, 10, and 20 mg/mL of $F_{0.30}$ and $AgF_{0.30}$, respectively; Images of nontreated HaCaT cells (CTRL) and cells treated with 4 mg/mL $F_{0.30}$ and $AgF_{0.30}$, immediately after, 24 h, and 48 h after the creation of the wound scratch (d); Quantification of the edge distance of the wound scratch at 0, 24, and 48 h

(e). $^{**}p < 0.01$ vs CTRL; Hemolytic percentage of $F_{0.30}$ and $AgF_{0.30}$. Normal saline and distilled water were used as the negative and positive control, respectively ($^{***}p < 0.001$) (f); Dynamic whole-blood-clotting evaluation of the $F_{0.30}$ and $AgF_{0.30}$ hydrogels and controls. A lower index value indicates a faster clotting rate. The absorbance of recalcified blood in deionized water was employed as control (g).

The blood clotting index (BCI) is a practical quantitative data to evaluate the coagulation performance of different materials. It is calculated from the absorbance (at 542 nm) of free hemoglobin not involved in the coagulation process, with a lower BCI indicating higher blood-clotting efficiency. Our results proved that blood in the control group did not spontaneously form clots and remained as a free-flowing liquid (Figure 5g). A significant difference ($p < 0.001$) was noticed between all the hydrogels ($F_{0.30}$ and $AgF_{0.30}$, 100 and 200 µL) and the control samples after being incubated with whole blood for 15, 30, and 60 minutes. Moreover, between the proposed hydrogels, a substantially enhanced blood clotting ability was primarily benefited from the introduction of AgNPs. In particular, samples with 100 µL volume of $AgF_{0.30}$ had the lowest coagulation index after 60 minutes (17.8 ± 0.4 %). Similar results were obtained by Liu et al. after 15 minutes of blood incubation with modified hyaluronic acid-based sponges (BCI ~ 50%).[68] Moreover, the prepared hydrogels in this study exhibited a hemostatic performance

as good as a commercial gelatin sponge (BCI = 33% after 15 min), analyzed by Liu et al. in their recent work.[72]

2.6 *In vivo* studies

The wound healing capacity of $F_{0.30}$ and $AgF_{0.30}$ hydrogels were evaluated using a full-thickness excisional wound-healing mice model, and the main results are shown in Figure 6. Specifically, in Figure 6a, photographs of wounds for the CTRL, $F_{0.30,}$ and $AgF_{0.30}$ mice are shown. The quantification of the wound closure rate is displayed in Figure 6b. $F_{0.30}$ and $AgF_{0.30}$ had a statistically higher closure rate compared to the CTRL after day 7 and day 3, respectively. At day 10, only $AgF_{0.30}$ produced a significant fasted healing of the wound with respect to the CTRL mice. Histological analysis of the collected tissues from CTRL, $F_{0.30,}$ and $AgF_{0.30}$ mice confirmed a different state in the healing progression. Specifically, histological images at 10 days shown in Figure 6c ensure earlier wound closure in the presence of the materials with increased presence of ECM and reduced distance between the two epithelial neo-migration tongues in $F_{0.30}$ and $AgF_{0.30}$-treated mice (Figure 6d).

A healing tissue synthesizes collagen, which is a constituent of growing cells. Hydroxyproline is a non-essential amino acid found in collagen. Therefore, the concentration

of hydroxyproline is a direct measure of the concentration of collagen. To this aim, hydroxyproline levels were quantified in the extracts of healing skin tissues from untreated and treated mice 7 days after injury (Figure 6e). In $F_{0.30}$ and $AgF_{0.30}$-treated mice, the hydroxyproline content was significantly increased compared to untreated mice.

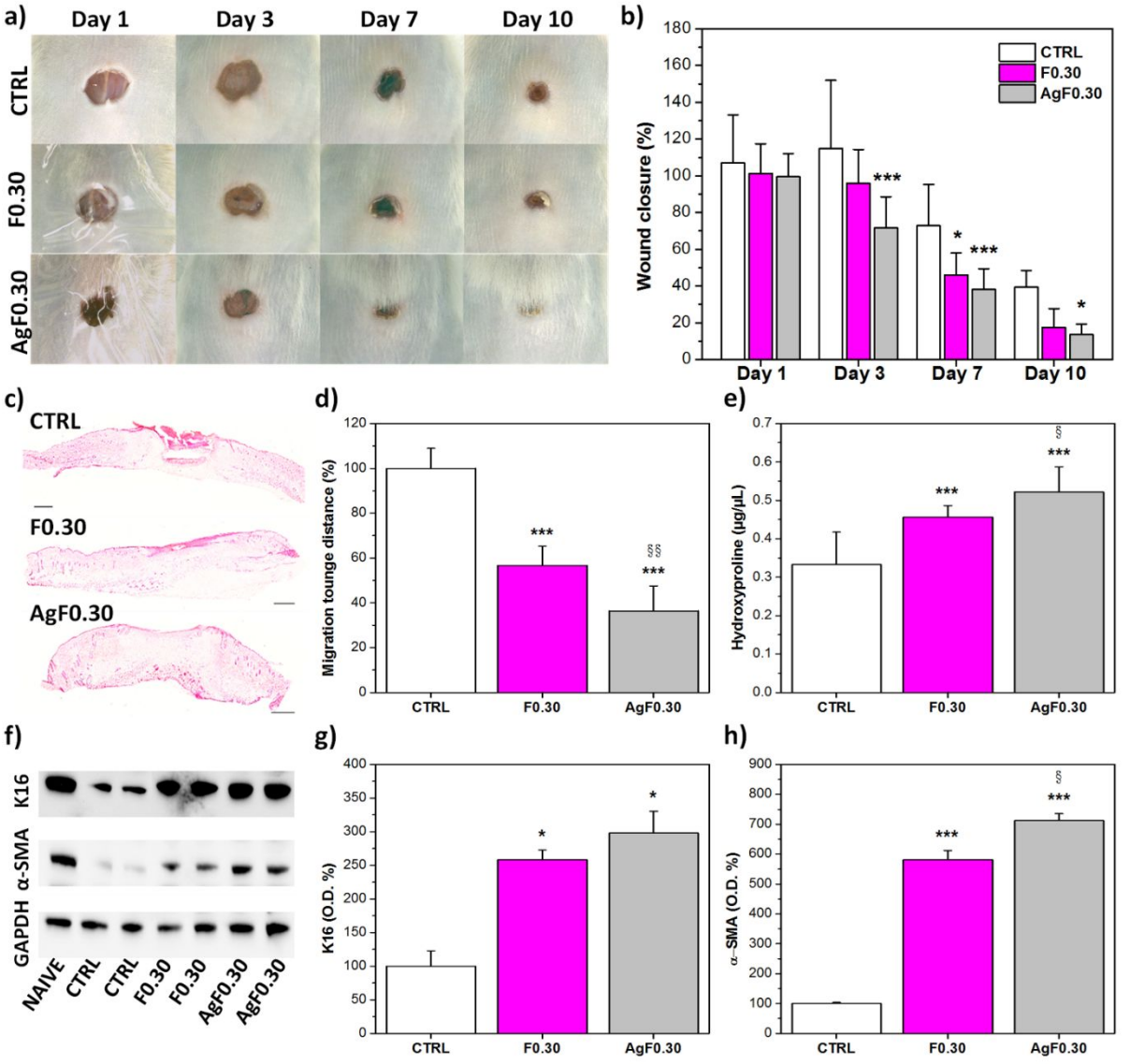

Figure 6. *In vivo* studies results. (a) Representative photographs of the skin of wounded mice at different time points (day 0, day 3, day 7, and day 10): control (CTRL), treated with $F_{0.30}$, treated with $AgF_{0.30}$. (b) Time-course (days) of wound healing in CTRL, $F_{0.30}$, and $AgF_{0.30}$ mice. (c) Hematoxylin-eosin staining of skin sections from the wound of CTRL, $F_{0.30}$, and $AgF_{0.30}$ mice (scale bars, 500 μm). Photo merge and reposition of multiple images. Skin sections were prepared 10 days after wound induction. (d) Percentage of migrating tongues distance for the wound of CTRL, $F_{0.30}$, and $AgF_{0.30}$ mice. (e) Quantification of produced hydroxyproline 7 days after wound induction for CTRL, $F_{0.30}$, $AgF_{0.30}$ mice. (f) Representative Western blot picture of K16 and α-SMA proteins in Naïve, CTRL, $F_{0.30}$, and $AgF_{0.30}$ mice. The blot is representative of 3 different analyses and illustrates the K16 and α-SMA protein expressions 7 days after wound induction. GAPDH was used as an internal control. Protein weights are expressed in kDa. (g, h) Percentage expression of K16 and α-SMA proteins in CTRL, $F_{0.30}$, and $AgF_{0.30}$ mice, respectively. * $p < 0.05$, ** $p < 0.01$, and *** $p < 0.001$, compared to CTRL. § $p < 0.05$, and §§ $p < 0.01$, compared to $F_{0.30}$.

During the healing process, activated fibroblasts are transformed into myofibroblasts, which modulate the production of the connective tissue and the expression of α-SMA.[73] Similarly, activated keratinocytes start producing different types of keratin to support the growth of the

new tissue; among them, K16 has a crucial role as a component of the keratin filament and cell adhesion.[74] After 7 days, the wound was induced and the levels of these two proteins were measured by Western blot. The blot and the results are reported in Figure 6f, 6g, and 6h, respectively. Both proteins are increased in the wound of animals treated with $F_{0.30}$ and $AgF_{0.30}$, indicating a higher proliferative closing activity than in mice without treatment.

Our findings demonstrate an overall improved condition of the wounds treated with the proposed hydrogels. Specifically, the $AgF_{0.30}$ treated wounds presented a more advanced state of histological condition after 10 days and increased in collagen production, activated fibroblasts, and keratinocytes after 7 days, compared to the control group.

3. CONCLUSIONS

Considering the uncountable advantages that hydrogels with self-healing properties can offer in biomedical applications, in this work, hydrogels based on two hyaluronic acid derivatives were developed entrapping AgNPs fabricated by the HA-DETA derivative, eliminating the need of toxic reducing agents. The DETA portion has multiple roles to participate in imine formation and exploit both reducing and stabilizing agents, enabling efficient binding and

controlled release of the nanoparticles. This extraordinary capping ability had a crucial impact in mitigating the toxicity of AgNPs.

The resulting Schiff base-based hydrogels are strongly influenced by pH. Since the infection would acidify the wound environment, these hydrogels accelerate the release of silver ions to execute antibacterial activity. Moreover, the HA-DETA derivative's itself intrinsic pH responsiveness intensifies the pH-responsive release mechanism, highlighting the on-demand and controlled antibacterial effect.

Noteworthy self-healing properties, with the ability of the hydrogel to repair after damage,due to body movement, further underscore the exceptional qualities of this antibacterial system proposed for wound healing, allowing complete contact with the injured site.

Finally, the *in vitro* and *in vivo* studies showed the excellent capacity of the $AgF_{0.30}$ hydrogel to increase the wound closure rate, promoting the deposition of ECM, production of collagen, and activation of fibroblasts and keratinocytes to obtain an overall ameliorated condition with respect to the control mice. Together, these results demonstrate that HA-DETA allows obtaining Ag-based hydrogels with optimal proprieties to be a new tool in treating infected and unhealed wounds.

4. EXPERIMENTAL SECTION

Materials: The hyaluronic acid (HA) 1000 kDa was purchased from Altergon, Italy. Ethylene glycol was purchased from Acros organics. The CellTiter 96# One Cell Proliferation Water Solution Assay (MTS) was purchased from Promega (Italy). Standard: solution of 32 components, 100 mg/L were purchased by CPACHEM - Ref N: 0C6A.K1.5N.L5.L5.

HaCaT cells were purchased from Cell Line Service (Heidelberg, Germany), 300493. CellTiter-Glo reagent was purchased from Promega (Madison, WI). C57BL/6J male mice were purchased from Charles River, Calco, Italy. All other materials were purchased from Sigma Aldrich.

Methods: Methods are reported in Supplementary Data section S.3.

HA-DETA and HA-Ald synthesis and characterization: HA-DETA was obtained, as reported elsewhere.[46] The degree of derivatization (DD%) was equal to 33 ± 3 mol%. HA-Ald was obtained by following the procedure as reported in the literature.[47] Weight-average molecular weight (Mw) was equal to 21.5 kDa and 1.1 polydispersity (PD).

The presence of aldehyde groups in Ha-Ald was confirmed by ^{1}H-NMR and by Fourier Transformed Infrared, data were collected on freeze-dried samples with attenuated total

reflectance (ATR FTIR), sample spectra were recorded in the spectral width region of 4000–500 cm^{-1}. To quantify the amount of aldehyde groups, a *tert*-butyl carbazate (t-BC) derivative of HA-Ald was obtained as reported by Ossipov et al. and ^{1}H-NMR was performed.[49]

HA-Ald/HA-DETA hydrogels production with or without AgNPs, preparation and characterization: Hydrogels were prepared in the same manner using HA-DETA with or without AgNPs. Nanocomposite HA-DETA/AgNPs dispersions were first obtained according to the reported procedure.[46] In particular, after complete dispersion, a freshly prepared solution of $AgNO_3$, was added to obtain HA-DETA 3% (w/v) and $AgNO_3$ (10 mM). The mixtures were placed under rapid stirring at room temperature for 1 minute and then irradiated with UV light generated by a high-pressure mercury lamp (365 nm and 100 W) for 30 minutes in a quartz tube. The color of the resulting solution changed to gray-brown after 30 minutes of UV irradiation, indicating the appearance of Ag nanoparticles. The sample obtained was labeled as Ag/HA-DETA.

HA-DETA or Ag/HA-DETA and HA-Ald were separately dispersed at 3% w/v in bi-distilled water; pH was adjusted to 7.4 with NaOH 0.1 M. HA-Ald was added in different molar ratios CHO/NH_2 to HA-DETA or Ag/HA-DETA, and vigorously mixed for few seconds.

Fourier Transform Infrared spectroscopy–attenuated total reflectance (FTIR–ATR) spectroscopy was carried out for all hydrogels after freeze-drying.

Gelation time was determined by the tube inversion method checking loss of fluidity of samples after mixing.

The crosslinking efficiency of HA-Ald/HA-DETA hydrogels was determined using the TNBS test.[75] To the freeze-dried products (8.34 mg, 7.14 mg, 6.67 mg and 5.56 mg of $F_{1.77}$, $F_{1.14}$, $F_{0.89}$ and $F_{0.30}$ respectively), $NaHCO_3$ (1 mL, 4% w/v) and TNBS solution (1 mL, 0.5% v/v) were added. The solution was mixed vigorously and kept at 60 °C for 4 hours. Subsequently, 3 mL of HCl 6 M were added to each sample and left at 40 °C for 90 minutes. The maximum absorbance of the trinitrophenyl complex formed using a UV-visible spectrophotometer at 420 nm was measured. The HA-DETA (5mg) was treated in the same way as control.

The crosslinking efficiency (ER%) was determined using the equation (1):

$$ER\% = \frac{Abs\ hydrogel}{Abs\ HA-DETA} * 100 \quad (1)$$

where Abs hydrogel corresponds to the absorbance of the tested hydrogels at different molar ratios ($F_{1.77}$, $F_{1.14}$, $F_{0.89,}$ and $F_{0.30}$) and Abs HA-DETA corresponds to the absorbance of the sample containing HA-DETA. AgNPs-loaded hydrogels were observed by SEM to evaluate the nanoparticles' distribution.

To perform rheological studies, Ag/HA-DETA (3% w/v) and HA-Ald (3% w/v) were mixed as described above, at different molar ratios, within the 48-well plate to obtain cylindrical hydrogels used for the analysis. Before each experiment, the sample was conditioned to the rheometer at 25 °C for 60 seconds. Strain sweep analysis from 0.1 to 1000 strain% was performed by applying a constant frequency of 0.1 Hz at 25 °C. The flow sweep experiment was conducted at 25 °C by applying a range from 0.01 to 100 s^{-1}.

The frequency sweep measurements were performed in a range of oscillation frequencies between 0.01 and 10 Hz, applying a constant strain of 1%.

The measurement gap was set at 1000 μm and the final volume of the hydrogel was 200 μL for all analyses. The excess sample was carefully removed before starting the experiment. All experiments were conducted using an 8 mm parallel plate with roughened surface.

Freeze-dried nanocomposite hydrogels ($n = 4$) prepared as described before were weighted and the initial weight was indicated as W_i. The scaffolds were soaked in 2 mL of phosphate buffer (pH 5.5 or 7.4) at 37 ˚C and the weight was recorded at selected time to measure its water absorption. At each time, scaffolds were washed in deionized water to remove any ions absorbed on the surface and the excess of water was removed gently with filter paper. The wet weight was recorded as W_s.

The rate of swelling of the scaffold was calculated using the following equation (2):

$$q\,ratio = \frac{W_s}{W_i} \quad (2)$$

In vitro degradability of samples (n = 4) was tested by incubating the freeze-dried scaffold in 2 mL of phosphate buffer (pH 5.5 or 7.4) at 37 ˚C and evaluating at the selected time the recovered weight of samples (W_r).

The rate of degradation was calculated using the following equation (3):

$$W_r\% = \frac{W_f}{W_i} \times 100 \quad (3)$$

where W_f is the weight of the recovered sample (final weight) at each set time, and W_i represents the initial weight.

The self-healing property of the AgNPs loaded hydrogels was examined by rheology measurements through recovery time studies. The storage and loss moduli were recorded at a frequency of 0.1 Hz under time sweep of 100 s with an alternate strain of 1% and 500% for 7 times. The self-healing properties were then macroscopically assayed. Briefly, two HA-Ald/HA-DETA hydrogels for each molar ratio were prepared. The polymer dispersions were previously colored by Azure II and Rhodamine B to obtain two hydrogel discs of different colors. Then the two hydrogels were spliced into two parts and placed in contact to assess their ability to completely reassemble at room temperature. After contact, hydrogels were observed

every 5 minutes. In addition, hydrogels were ground into pieces using a mortar and pestle and placed into the mold for reassembly.

To assess hydrogels' pH responsiveness, samples containing AgNPs were prepared as described above and immersed for 24 hours into phosphate buffer (pH 5.5 or 7.4). Frequency sweep analyses were performed on these samples using the parameters described above. Moreover, to assess the dynamics of the imine bond as a function of pH, HCl (1 M) was added by gently shaking to the hydrogels previously stained with Rhodamine B and Azure II. Then, an equivalent amount of NaOH (1 M) was added, neutralizing the acid. This process was repeated twice.

Ag ions release studies: The release of Ag^+ from hydrogels (200 µL), produced as described in the previous paragraph, was evaluated at pH 5.5 or 7.4. In particular, 9.8 mL of phosphate buffer at pH 5.5 or phosphate buffer at pH 7.4 were added to each hydrogel. The samples were incubated at 37 ˚C and at different contact times, namely 24, 48, 144, 288 and 480 hours for samples at pH 7.4, and 1, 3, 8 and 24 hours for samples at pH 5.5. The silver content of the supernatant treated with HNO_3 was analyzed by ICP-OES technique. Silver standard solutions in the concentration range 0.05 – 20 mg/L were used to calibrate the spectrophotometer before each set of measurements.

In vitro antibacterial activity: The microbial strains utilized in this study were sourced from the American Type Culture Collection (ATCC). Reference strains, *Pseudomonas aeruginosa* ATCC 15442 and *Staphylococcus aureus* ATCC 25923, were used for conducting the diffusion test and viable plate count, as outlined by Biscari et al. and Federico et al.[76,77] In the diffusion test, bacterial strains were cultivated in Tryptic Soy Agar (TSA) overnight at 37˚C. Bacterial suspensions were prepared in NaCl 0.9% (v/v) to achieve a cell density of 10^5 colony-forming units (CFU)/mL. Subsequently, 200 µL of a bacterial suspension was evenly spread onto an agar plate, followed by the placement of hydrogels onto the surface of the bacteria-containing plate. These plates were then incubated at 37˚C overnight, and after incubation, the inhibition zone surrounding the hydrogels was assessed.

To evaluate the inhibition of planktonic growth, we conducted viable plate counts of *P. aeruginosa* ATCC 15442 and *S. aureus* ATCC 25923 in the presence of hydrogels on Tryptic Soy Broth (TSB) medium at different pH values (5.5 and 7.4). Bacterial suspension at a concentration of 10^6 CFU/mL, were prepared.[78] Next, 25 µL of each bacterial culture were added to 24-well plates containing 2 mL of TSB at pH values of 5.5 or 7.4, along with unique hydrogels ($AgF_{1.77}$, $AgF_{1.14}$, $AgF_{0.89}$, and $AgF_{0.30}$). These plates were incubated at 37˚C under stationary conditions. Control wells were established, which included microorganisms without

hydrogels, to allow for comparison under identical experimental conditions. After 24 hours of incubation, 1 mL of bacterial suspension was extracted from each well and used for bacterial counting. In brief, the bacterial suspension was added to test tubes containing 9 mL of NaCl (0.9% w/v solution), and a number of 10-fold dilutions were prepared. Aliquots of 100 μL from each dilution were then plated onto TSA plates, which were subsequently incubated at 37˚C overnight. To quantify the number of viable bacteria in each system, we determined the CFU/mL value.

Cytocompatibility: In vitro biological studies were performed with normal human dermal fibroblasts (NHDF) and immortalized human keratinocyte cell line (HaCaT). Specifically, NHDF were cultivated in Dulbecco's Minimum Essential Medium (DMEM) enriched with 10% v/v fetal bovine serum (FBS), 1% v/v penicillin-streptomycin solution, 1 % v/v of glutamine solution and 0.1 % v/v of amphotericin B solution. The cells were kept in a flask containing 10 mL of culture medium and incubated at 37 °C in a humidified atmosphere containing 5 % of CO_2. After trypsinization, the cells were counted and suspended in DMEM. In particular, the cells were plated into a 48-well plate at the seeding density of 3×10^4 cells per well. After 24 hours, the cytocompatibility of the crosslinked HA-Ald/HA-DETA hydrogels

has been assessed. Specifically, hydrogels (100μL) with or without AgNPs were introduced into a BRAND insert in a 48-well plate containing 3 x 10^4 cells.

After 24 and 48 hours of incubation, cell viability was evaluated using the MTS colorimetric test (performed according to the protocol reported by the manufacturer). Absorbance at 492 nm was recorded by a UV-vis microplate reader and cell viability was expressed as a percentage of viability compared to incubated cells in the presence of culture medium, which were used as a negative control. Live and Dead assay was performed for AgNPs loaded hydrogels to distinguish alive and dead cells.

The same analysis was conducted by encapsulating the cells within hydrogels without AgNPs. Specifically, an appropriate volume of HA-DETA was placed inside the cover glass, followed by the addition of cells at a density of 1 x 10^5, mixing them, and then rapidly adding HA-Ald. After 1, 2 and 7 days of incubation, the samples were treated with the Live/Dead Kit, and visualization was performed using a fluorescence microscope.

HaCaT were cultured in DMEM supplemented with 10% fetal bovine serum (FBS) and 2 mmol/L L-glutamine at 37 ˚C in an atmosphere of 5% CO_2 and 95% air. The cytotoxicity assessment was conducted using CellTiter Glo Luminescent viability assay. HaCaT cells were placed in 96-well plates at a density of 3.5 × 10^5 in a final medium well volume of 100 μL and

incubated until the proper confluence was reached. After 24 h of treatment, cells were quickly rinsed with pre-warmed PBS with Ca^{2+}/Mg^{2+}, and the extraction medium was substituted with the extraction one (control samples were treated with medium processed as the extractions). Afterwards, cells were incubated for an additional 24 h and 48 h. Extracts were produced by placing hydrogels $F_{0.30}$ and $AgF_{0.30}$ in cell medium at different concentrations. According to ISO10993-5 guidelines, as the cell viability of the sample extracts were higher than 70% of the control group, all materials were considered biocompatible. Cell viability was determined by measuring ATP levels by CellTiter-Glo assay, as indicated by the supplier as percentage survival relative to control cells.

All samples, before cytocompatibility studies were sterilized by UV radiation at 254 nm for 20 minutes, using a 125 W UV lamp.

In vitro wound scratch assay: Keratinocytes (HaCaT cell lines) were seeded into 24-well plates at 30×10^4 cells and were maintained at 37 ˚C and 5% CO_2 for 24 h to permit cell adhesion and the formation of a confluent monolayer. Subsequently, they were wounded with a sterile plastic pipette tip to leave a scratch of approximately 0.4 mm in width. The cells were then washed twice with phosphate-buffered saline (PBS), and medium was replaced by the extracts of the hydrogels. Wound closure was monitored, collecting digitized images

immediately after scratching, 24 h and 48 h post-induction. Images were analyzed using ImageJ software (National Institute of Health, USA). Data has been reported as the extent of wound closure by the initial scratch width.

Hemocompatibility evaluation with mouse whole blood: Hemocompatibility tests were performed to determine the blood compatibility of the proposed hydrogels ($F_{0.30}$) with and without AgNPs for wound treatment, according to the ISO 10993-4 standard. C57BL/6 mice weighing 22−24 g were used (Charles River, Calco, Italy) and all procedures were performed following the Ethical Guidelines of the European Communities Council (Directive 2010/63/EU) and accepted by the Italian Ministry of Health (746/2019-PR). According to the "3Rs concept", every attempt was made to reduce animal suffering and to utilize the fewest number of animals necessary to provide accurate findings. Healthy mouse blood containing heparin (5000 U/mL) was taken and diluted with normal saline (4:5 ratio by volume), following standard procedures.[79] Fresh heparinized blood was stored at room temperature and used within 2 hours of collection.

Hemolysis assay: Hydrogels $F_{0.30}$ (100 µL or 200 µL as final volume, with and without AgNPs) were individually prepared and placed in a 24-well plate. Hydrogels were quickly rinsed in PBS, soaked in 1.5 mL of normal physiological saline, and kept at 37˚C for 30

minutes. Normal physiological saline and distilled water served as negative and positive controls. After that, 0.03 mL of diluted blood was added to the hydrogel surfaces or the wells with no hydrogel. Samples were incubated at 37˚C for another 60 minutes. All the volume of each well was withdrawn, centrifuged at 3000 rpm for 5 min at room temperature, and the supernatant (100 μL) was transferred to a 96-well plate. The absorbance at 542 nm was recorded using a microplate reader.

The percentage of hemolysis (HR) was calculated by the following equation (4):

$$HR\% = (A - Aneg)/(Apos - Aneg) \times 100 \quad (4)$$

where A is the absorbance of the test well, Aneg the absorbance of the well with normal saline (negative control), and Apos the absorbance of the well with distilled water (positive control).

Blood Clotting: Hydrogels $F_{0.30}$ (100 μL or 200 μL as final volume, with and without AgNPs) were individually placed into a 24-well plate and prewarmed at 37˚C for 5 minutes. Afterward, 100 μL of blood sample was slowly added to the hydrogel surface, followed by $CaCl_2$ solution (0.2 M, 10 μL) to start the coagulation process. Wells without hydrogels were used as controls. After incubating the samples at 37 ˚C for 15 min, 30 min, and 60 min, 2 mL of deionized water were carefully added to the wells along the inside wall. The plate was shaken for 1 min, and

subsequently, the solutions were transferred into a 96-well plate. A microplate reader measured the absorbance of the samples at 542 nm.

The blood clotting index (BCI) of the samples was calculated by the following equation (5):

$$BCI(\%) = {}^{Ih}/_{Ic} * 100 \quad (5)$$

where I_h is the absorbance of blood that had contact with the sample, and I_c is the absorbance of blood hemolyzed with deionized water at the first time point.

In vivo studies

Animals: In vivo experiments were performed as already reported in *Hemocompatibility evaluation with mouse whole blood* section. They were kept under a 12-h light/dark cycle (lights on at 8:00 am), relative humidity of (55 ± 10%), and at a controlled temperature of 21 ± 1 ˚C.

Wound Closure: For the evaluation of the wound closure, mice (n = 5 for each group) were anesthetized, their dorsal surface was shaved, and a full-thickness excisional wound was induced (diameter 6 mm). A photo of the wound was taken immediately after the biopsy generation (day 1). 40 mg of HA and HA-Ag hydrogels were applied, and pictures at days 1, 3, 7, and 10 were collected and analyzed using ImageJ software to quantify the wound closure rate. The wound closure was calculated as a percentage based on wound size relative to the

control group. During the experiments, mice were housed individually and fed with water and food ad libitum.

Histology: After 10 days from wound induction, skin samples were excised and fixed in 10% formalin solution and embedded in paraffin. Serial sections of 5-μm thickness were obtained and stained with Hematoxylin & Eosin (H&E) to evaluate morphology and analyzed with a Leica DM5500 optical microscope (n = 5 each group). Migration tongue distance variation was expressed as an absolute distance in μm vs. control group (tip distance was measured with ImageJ software). The results were examined blindly.

Hydroxyproline production measurements: Hydroxyproline (4-hydroxyproline) production was evaluated in a skin biopsy from untreated, $F_{0.30}$, $AgF_{0.30}$ treated animals collected 7 days post wound induction and snap-frozen in liquid nitrogen (n = 5 mice each experimental group). By using hydroxyproline assay kit (Sigma Aldrich), according to the manufacturer's instructions, the amount of hydroxyproline was calculated as μg/μL of hydroxyproline per full thickness skin biopsy.

Western blot: Mice skin samples (n = 5 for each group) were taken after 7 days and homogenized in lysis buffer (150 mM sodium chloride, 50 mM Tris·HCl, pH 8.0, 0.5% sodium deoxycholate, 0.1% SDS, and 1% Triton X-100). The tissue extracts were cleaned by

centrifugation (15 min at 12000 × g, 4 ˚C). Proteins (30 μg) were separated by SDS/PAGE and transferred to nitrocellulose membranes. The membranes were blocked with 5% not fat dry milk in Tris-buffered saline (TBS) and incubated overnight with anti–K16 antibody (1:500; Abcam) and anti-α-SMA antibody (1:500; Abcam) in TBS containing 1% nonfat dry milk, followed by incubation with secondary antibodies. Finally, proteins were visualized with a chemiluminescence kit (Bio-Rad), and images were obtained by using a lumino-image analyzing system (Bio-Rad). Quantification was performed by using ImageJ software.

Statistical analysis: All results are reported with a media ± standard deviation (n=3 if not otherwise stated) and, when applicable the statistical analysis for significance was conducted with the Student's t-test, using the function t-test of Microsoft Excel, assuming the not homogenous variance at 2 samples and a dual tile distribution; values with $p < 0.05$ were considered statistically significant.

In the wound scratch assay and *in vivo* analyses, ANOVA was utilized to evaluate statistical significance, followed by Bonferroni's post-hoc test. GraphPad Prism 5 was utilized for all statistical analysis (GraphPad Software Inc., San Diego, CA, USA). Results with a *p-value* < 0.05 were considered statistically significant.

ASSOCIATED CONTENT

Supporting Information

The Supporting Information is available free of charge on the ACS Publications website. Details and additional figures about characterization of polymer derivatives and hydrogels. Methods.

AUTHOR INFORMATION

Corresponding Author

*Fabio S. Palumbo: Department of Biological, Chemical, and Pharmaceutical Sciences and Technologies (STEBICEF), University of Palermo, Via Archirafi 32, 90123 Palermo, Italy

Email: fabiosalvatore.palumbo@unipa.it

*Martina Lenzuni: Smart Materials, Istituto Italiano di Tecnologia, Via Morego 30, 16163, Genova, Italy

Email: martina.lenzuni@edu.unige.it

*Marco Contardi: Smart Materials, Istituto Italiano di Tecnologia, Via Morego 30, 16163, Genova, Italy

Email: marco.contardi@iit.it

Present Addresses

Martina Lenzuni: †Department of Civil, Chemical and Environmental Engineering, University of Genoa, Via All'Opera Pia 15, 16145, Genova, Italy.

Author Contributions

The manuscript was written through contributions of all authors. All authors have given approval to the final version of the manuscript. §Co-last authors

Notes

The authors declare no conflict of interest.

REFERENCES

(1) Patenaude, M.; Smeets, N. M. B.; Hoare, T. Designing Injectable, Covalently Cross-Linked Hydrogels for Biomedical Applications. *Macromol. Rapid Commun.* 2014, *35* (6), 598–617.

(2) Pitarresi, G.; Palumbo, F. S.; Fiorica, C.; Bongiovì, F.; Martorana, A.; Federico, S.; Chinnici, C. M.; Giammona, G. Composite Hydrogels of Alkyl Functionalized Gellan Gum Derivative and Hydroxyapatite/Tricalcium Phosphate Nanoparticles as Injectable Scaffolds for

Bone Regeneration. *Macromol. Biosci.* **2022**, *22* (2), 2100290.

(3) Sivashanmugam, A.; Arun Kumar, R.; Vishnu Priya, M.; Nair, S. V.; Jayakumar, R. An Overview of Injectable Polymeric Hydrogels for Tissue Engineering. *Eur. Polym. J.* **2015**, *72*, 543–565.

(4) Sun, Y.; Nan, D.; Jin, H.; Qu, X. Recent Advances of Injectable Hydrogels for Drug Delivery and Tissue Engineering Applications. *Polym. Test.* **2020**, *81*, 106283.

(5) Mo, C.; Xiang, L.; Chen, Y. Advances in Injectable and Self-Healing Polysaccharide Hydrogel Based on the Schiff Base Reaction. *Macromol. Rapid Commun.* **2021**, *42* (10), 2100025.

(6) Singh, M. R.; Patel, S.; Singh, D. Natural Polymer-Based Hydrogels as Scaffolds for Tissue Engineering. *Nanobiomaterials Soft Tissue Eng. Appl. Nanobiomaterials* **2016**, 231–260.

(7) Francis Suh, J. K.; Matthew, H. W. T. Application of Chitosan-Based Polysaccharide Biomaterials in Cartilage Tissue Engineering: A Review. *Biomaterials* **2000**, *21* (24), 2589–2598.

(8) Pita-López, M. L.; Fletes-Vargas, G.; Espinosa-Andrews, H.; Rodríguez-Rodríguez, R.

Physically Cross-Linked Chitosan-Based Hydrogels for Tissue Engineering Applications: A State-of-the-Art Review. *Eur. Polym. J.* **2021**, *145*, 110176.

(9) Pitarresi, G.; Martorana, A.; Palumbo, F. S.; Fiorica, C.; Giammona, G. New Gellan Gum-Graft-Poly(d,l-Lactide-Co-Glycolide) Copolymers as Promising Bioinks: Synthesis and Characterization. *Int. J. Biol. Macromol.* **2020**, *162*, 1653–1667.

(10) Patel, M. A.; AbouGhaly, M. H. H.; Schryer-Praga, J. V.; Chadwick, K. The Effect of Ionotropic Gelation Residence Time on Alginate Cross-Linking and Properties. *Carbohydr. Polym.* **2017**, *155*, 362–371.

(11) Li, L.; Yan, B.; Yang, J.; Chen, L.; Zeng, H. Novel Mussel-Inspired Injectable Self-Healing Hydrogel with Anti-Biofouling Property. *Adv. Mater.* **2015**, *27* (7), 1294–1299.

(12) Lai, W. F. Development of Hydrogels with Self-Healing Properties for Delivery of Bioactive Agents. *Mol. Pharm.* **2021**, *18* (5), 1833–1841.

(13) Saunders, L.; Ma, P. X. Self-Healing Supramolecular Hydrogels for Tissue Engineering Applications. *Macromol. Biosci.* **2019**, *19* (1), 1800313.

(14) Anupama Devi, V. K.; Shyam, R.; Palaniappan, A.; Jaiswal, A. K.; Oh, T. H.; Nathanael, A. J. Self-Healing Hydrogels: Preparation, Mechanism and Advancement in

Biomedical Applications. *Polym. 2021, Vol. 13, Page 3782* **2021**, *13* (21), 3782.

(15) Zhang, W.; Zhang, K.; Yan, S.; Wu, J.; Yin, J. A Tough and Self-Healing Poly(L-Glutamic Acid)-Based Composite Hydrogel for Tissue Engineering. *J. Mater. Chem. B* **2018**, *6* (42), 6865–6876.

(16) Chai, Q.; Jiao, Y.; Yu, X. Hydrogels for Biomedical Applications: Their Characteristics and the Mechanisms behind Them. *Gels 2017, Vol. 3, Page 6* **2017**, *3* (1), 6.

(17) Tong, Z.; Jin, L.; Oliveira, J. M.; Reis, R. L.; Zhong, Q.; Mao, Z.; Gao, C. Adaptable Hydrogel with Reversible Linkages for Regenerative Medicine: Dynamic Mechanical Microenvironment for Cells. *Bioact. Mater.* **2021**, *6* (5), 1375–1387.

(18) Li, X.; Sun, Q.; Li, Q.; Kawazoe, N.; Chen, G. Functional Hydrogels with Tunable Structures and Properties for Tissue Engineering Applications. *Front. Chem.* **2018**, *6* (OCT), 499.

(19) Qu, J.; Zhao, X.; Liang, Y.; Zhang, T.; Ma, P. X.; Guo, B. Antibacterial Adhesive Injectable Hydrogels with Rapid Self-Healing, Extensibility and Compressibility as Wound Dressing for Joints Skin Wound Healing. *Biomaterials* **2018**, *183*, 185–199.

(20) Chen, G.; Yu, Y.; Wu, X.; Wang, G.; Ren, J.; Zhao, Y. Bioinspired Multifunctional

Hybrid Hydrogel Promotes Wound Healing. *Adv. Funct. Mater.* 2018, *28* (33), 1801386.

(21) Mohamed, A. L.; Elmotasem, H.; Salama, A. A. A. Colchicine Mesoporous Silica Nanoparticles/Hydrogel Composite Loaded Cotton Patches as a New Encapsulator System for Transdermal Osteoarthritis Management. *Int. J. Biol. Macromol.* 2020, *164*, 1149–1163.

(22) Wang, Y.; Adokoh, C. K.; Narain, R. Recent Development and Biomedical Applications of Self-Healing Hydrogels. *Expert Opin. Drug Delivery.* 2018, *15* (1), 77–91.

(23) Sharma, S.; Jain, P.; Tiwari, S. Dynamic Imine Bond Based Chitosan Smart Hydrogel with Magnified Mechanical Strength for Controlled Drug Delivery. *Int. J. Biol. Macromol.* 2020, *160*, 489–495.

(24) Qian, C.; Zhang, T.; Gravesande, J.; Baysah, C.; Song, X.; Xing, J. Injectable and Self-Healing Polysaccharide-Based Hydrogel for PH-Responsive Drug Release. *Int. J. Biol. Macromol.* 2019, *123*, 140–148.

(25) Qian, Z.; Wang, H.; Bai, Y.; Wang, Y.; Tao, L.; Wei, Y.; Fan, Y.; Guo, X.; Liu, H. Improving Chronic Diabetic Wound Healing through an Injectable and Self-Healing Hydrogel with Platelet-Rich Plasma Release. *ACS Appl. Mater. Interfaces* 2020, *12* (50), 55659–55674.

(26) Martorana, A.; Pitarresi, G.; Palumbo, F. S.; Barberi, G.; Fiorica, C.; Giammona, G.

Correlating Rheological Properties of a Gellan Gum-Based Bioink: A Study of the Impact of Cell Density. *Polym. 2022, Vol. 14, Page 1844* **2022**, *14* (9), 1844.

(27) Trask, R. S.; Williams, H. R.; Bond, I. P. Self-Healing Polymer Composites: Mimicking Nature to Enhance Performance. *Bioinspir. Biomim.* **2007**, *2* (1), P1.

(28) McKay, C. S.; Finn, M. G. Click Chemistry in Complex Mixtures: Bioorthogonal Bioconjugation. *Chem. Biol.* **2014**, *21* (9), 1075–1101.

(29) Lü, S.; Gao, C.; Xu, X.; Bai, X.; Duan, H.; Gao, N.; Feng, C.; Xiong, Y.; Liu, M. Injectable and Self-Healing Carbohydrate-Based Hydrogel for Cell Encapsulation. *ACS Appl. Mater. Interfaces* **2015**, *7* (23), 13029–13037.

(30) Wang, C.; Liang, C.; Wang, R.; Yao, X.; Guo, P.; Yuan, W.; Liu, Y.; Song, Y.; Li, Z.; Xie, X. The Fabrication of a Highly Efficient Self-Healing Hydrogel from Natural Biopolymers Loaded with Exosomes for the Synergistic Promotion of Severe Wound Healing. *Biomater. Sci.* **2019**, *8* (1), 313–324.

(31) Sharma, P. K.; Singh, Y. Glyoxylic Hydrazone Linkage-Based PEG Hydrogels for Covalent Entrapment and Controlled Delivery of Doxorubicin. *Biomacromolecules* **2019**, *20* (6), 2174–2184.

(32) Jiang, X.; Yang, X.; Yang, B.; Zhang, L.; Lu, A. Highly Self-Healable and Injectable Cellulose Hydrogels via Rapid Hydrazone Linkage for Drug Delivery and 3D Cell Culture. *Carbohydr. Polym.* **2021**, *273*, 118547.

(33) Zhao, F.; Liu, Y.; Song, T.; Zhang, B.; Li, D.; Xiao, Y.; Zhang, X. A Chitosan-Based Multifunctional Hydrogel Containing in Situ Rapidly Bioreduced Silver Nanoparticles for Accelerating Infected Wound Healing. *J. Mater. Chem. B* **2022**, *10* (13), 2135–2147.

(34) Schneider, L. A.; Korber, A.; Grabbe, S.; Dissemond, J. Influence of PH on Wound-Healing: A New Perspective for Wound-Therapy? *Arch. Dermatol. Res.* **2007**, *298* (9), 413–420.

(35) Wu, Y.; Wang, Y.; Long, L.; Hu, C.; Kong, Q.; Wang, Y. A Spatiotemporal Release Platform Based on PH/ROS Stimuli-Responsive Hydrogel in Wound Repairing. *J. Control. Release* **2022**, *341*, 147–165.

(36) Pitarresi, G.; Barberi, G.; Palumbo, F. S.; Schillaci, D.; Fiorica, C.; Catania, V.; Indelicato, S.; Bongiorno, D.; Biscari, G.; Giammona, G. Developing Antibiofilm Fibrillar Scaffold with Intrinsic Capacity to Produce Silver Nanoparticles. *Int. J. Mol. Sci.* **2022**, *23* (23), 15378.

(37) Liu, X.; Zhou, S.; Cai, B.; Wang, Y.; Deng, D.; Wang, X. An Injectable and Self-Healing Hydrogel with Antibacterial and Angiogenic Properties for Diabetic Wound Healing. *Biomater. Sci.* 2022, *10* (13), 3480–3492.

(38) Chai, C.; Zhang, P.; Ma, L.; Fan, Q.; Liu, Z.; Cheng, X.; Zhao, Y.; Li, W.; Hao, J. Regenerative Antibacterial Hydrogels from Medicinal Molecule for Diabetic Wound Repair. *Bioact. Mater.* 2022.

(39) Mohammed, Z. S.; Lataef, R.; Alwash, S. W.; Sultan, S. J.; Mohammed, N. M.; Abed, A. S. Investigation on the Possible Cutaneous Toxicity of Silver Nanoparticles in Swiss Albino Rats. *J. Nanostructures* 2022, *12* (3), 754–760.

(40) Jiang, Y.; Huang, J.; Wu, X.; Ren, Y.; Li, Z.; Ren, J. Controlled Release of Silver Ions from AgNPs Using a Hydrogel Based on Konjac Glucomannan and Chitosan for Infected Wounds. *Int. J. Biol. Macromol.* 2020, *149*, 148–157.

(41) Yan, K.; Xu, F.; Wei, W.; Yang, C.; Wang, D.; Shi, X. Electrochemical Synthesis of Chitosan/Silver Nanoparticles Multilayer Hydrogel Coating with PH-Dependent Controlled Release Capability and Antibacterial Property. *Colloids Surfaces B Biointerfaces* 2021, *202*, 111711.

(42) Deka, R.; Boruah, P.; Ali, A. A.; Dutta, R.; Gogoi, P.; Sarmah, J. K. Smart Hydrogel with Rapid Self-Healing and Controlled Release Attributes for Biomedical Applications. *Smart Mater. Struct.* **2022**, *31* (9), 095039.

(43) Dovedytis, M.; Liu, Z. J.; Bartlett, S. Hyaluronic Acid and Its Biomedical Applications: A Review. *Eng. Regen.* **2020**, *1*, 102–113.

(44) Owen, S. C.; Fisher, S. A.; Tam, R. Y.; Nimmo, C. M.; Shoichet, M. S. Hyaluronic Acid Click Hydrogels Emulate the Extracellular Matrix. *Langmuir* **2013**, *29* (24), 7393–7400.

(45) Neuman, M. G.; Nanau, R. M.; Oruña-Sanchez, L.; Coto, G. Hyaluronic Acid and Wound Healing. *J. Pharm. Pharm. Sci.* **2015**, *18* (1), 53–60.

(46) Martorana, A.; Pitarresi, G.; Palumbo, F. S.; Catania, V.; Schillaci, D.; Mauro, N.; Fiorica, C.; Giammona, G. Fabrication of Silver Nanoparticles by a Diethylene Triamine-Hyaluronic Acid Derivative and Use as Antibacterial Coating. *Carbohydr. Polym.* **2022**, *295*, 119861.

(47) Su, W.-Y.; Chen, Y.-C.; Lin, F.-H. Injectable Oxidized Hyaluronic Acid/Adipic Acid Dihydrazide Hydrogel for Nucleus Pulposus Regeneration. *Acta Biomater.* **2010**, *6* (8), 3044–3055.

(48) Banerjee, S. L.; Singha, N. K. A New Class of Dual Responsive Self-Healable Hydrogels Based on a Core Crosslinked Ionic Block Copolymer Micelle Prepared via RAFT Polymerization and Diels–Alder "Click" Chemistry. *Soft Matter* **2017**, *13* (47), 9024–9035.

(49) Ossipov, D. A.; Yang, X.; Varghese, O.; Kootala, S.; Hilborn, J. Modular Approach to Functional Hyaluronic Acid Hydrogels Using Orthogonal Chemical Reactions. *Chem. Commun.* **2010**, *46* (44), 8368–8370.

(50) Xiong, J.; Wu, X. dong; Xue, Q. ji. One-Step Synthesis of Highly Monodisperse Silver Nanoparticles Using Poly-Amino Compounds. *Colloids Surfaces A Physicochem. Eng. Asp.* **2014**, *441*, 109–115.

(51) Alarcon, E. I.; Udekwu, K.; Skog, M.; Pacioni, N. L.; Stamplecoskie, K. G.; González-Béjar, M.; Polisetti, N.; Wickham, A.; Richter-Dahlfors, A.; Griffith, M.; Scaiano, J. C. The Biocompatibility and Antibacterial Properties of Collagen-Stabilized, Photochemically Prepared Silver Nanoparticles. *Biomaterials* **2012**, *33* (19), 4947–4956.

(52) Wang, Y.; Xie, R.; Li, Q.; Dai, F.; Lan, G.; Shang, S.; Lu, F. A Self-Adapting Hydrogel Based on Chitosan/Oxidized Konjac Glucomannan/AgNPs for Repairing Irregular Wounds. *Biomater. Sci.* **2020**, *8* (7), 1910–1922.

(53) Qu, J.; Zhao, X.; Ma, P. X.; Guo, B. PH-Responsive Self-Healing Injectable Hydrogel Based on N-Carboxyethyl Chitosan for Hepatocellular Carcinoma Therapy. *Acta Biomater.* **2017**, *58*, 168–180.

(54) Guvendiren, M.; Lu, H. D.; Burdick, J. A. Shear-Thinning Hydrogels for Biomedical Applications. *Soft Matter* **2011**, *8* (2), 260–272.

(55) Pang, Y.; Liu, J.; Moussa, Z. L.; Collins, J. E.; McDonnell, S.; Hayward, A. M.; Jajoo, K.; Langer, R.; Traverso, G. Endoscopically Injectable Shear-Thinning Hydrogels Facilitating Polyp Removal. *Adv. Sci.* **2019**, *6* (19).

(56) Mondal, P.; Chatterjee, K. Injectable and Self-Healing Double Network Polysaccharide Hydrogel as a Minimally-Invasive Delivery Platform. *Carbohydr. Polym.* **2022**, *291*, 119585.

(57) Wei, Z.; Yang, J. H.; Liu, Z. Q.; Xu, F.; Zhou, J. X.; Zrínyi, M.; Osada, Y.; Chen, Y. M. Novel Biocompatible Polysaccharide-Based Self-Healing Hydrogel. *Adv. Funct. Mater.* **2015**, *25* (9), 1352–1359.

(58) Li, S.; Pei, M.; Wan, T.; Yang, H.; Gu, S.; Tao, Y.; Liu, X.; Zhou, Y.; Xu, W.; Xiao, P. Self-Healing Hyaluronic Acid Hydrogels Based on Dynamic Schiff Base Linkages as Biomaterials. *Carbohydr. Polym.* **2020**, *250* (May), 116922.

(59) Yang, B.; Zhang, Y.; Zhang, X.; Tao, L.; Li, S.; Wei, Y. Facilely Prepared Inexpensive and Biocompatible Self-Healing Hydrogel: A New Injectable Cell Therapy Carrier. *Polym. Chem.* **2012**, *3* (12), 3235–3238.

(60) Wu, M.; Chen, J.; Huang, W.; Yan, B.; Peng, Q.; Liu, J.; Chen, L.; Zeng, H. Injectable and Self-Healing Nanocomposite Hydrogels with Ultrasensitive PH-Responsiveness and Tunable Mechanical Properties: Implications for Controlled Drug Delivery. *Biomacromolecules* **2020**, *21* (6), 2409–2420.

(61) Diban, F.; Di Lodovico, S.; Di Fermo, P.; D'Ercole, S.; D'Arcangelo, S.; Di Giulio, M.; Cellini, L. Biofilms in Chronic Wound Infections: Innovative Antimicrobial Approaches Using the In Vitro Lubbock Chronic Wound Biofilm Model. *Int. J. Mol. Sci.* **2023**, *24* (2).

(62) Zhao, G.; Usui, M. L.; Lippman, S. I.; James, G. A.; Stewart, P. S.; Fleckman, P.; Olerud, J. E. Biofilms and Inflammation in Chronic Wounds. *Adv. Wound Care* **2013**, *2* (7), 389.

(63) Liu, H.; Li, Z.; Che, S.; Feng, Y.; Guan, L.; Yang, X.; Zhao, Y.; Wang, J.; Zvyagin, A. V.; Yang, B.; Lin, Q. A Smart Hydrogel Patch with High Transparency, Adhesiveness and Hemostasis for All-Round Treatment and Glucose Monitoring of Diabetic Foot Ulcers. *J.*

Mater. Chem. B 2022, *10* (30), 5804–5817.

(64) Shah, S. A.; Sohail, M.; Khan, S.; Minhas, M. U.; de Matas, M.; Sikstone, V.; Hussain, Z.; Abbasi, M.; Kousar, M. Biopolymer-Based Biomaterials for Accelerated Diabetic Wound Healing: A Critical Review. *Int. J. Biol. Macromol.* 2019, *139*, 975–993.

(65) Wang, L.; Zhang, D.; Ren, Y.; Guo, S.; Li, J.; Ma, S.; Yao, M.; Guan, F. Injectable Hyaluronic Acid Hydrogel Loaded with BMSC and NGF for Traumatic Brain Injury Treatment. *Mater. Today Bio* 2022, *13*, 100201.

(66) Sagbas Suner, S.; Ari, B.; Onder, F. C.; Ozpolat, B.; Ay, M.; Sahiner, N. Hyaluronic Acid and Hyaluronic Acid: Sucrose Nanogels for Hydrophobic Cancer Drug Delivery. *Int. J. Biol. Macromol.* 2019, *126*, 1150–1157.

(67) Liang, Y.; Zhao, X.; Hu, T.; Chen, B.; Yin, Z.; Ma, P. X.; Guo, B. Adhesive Hemostatic Conducting Injectable Composite Hydrogels with Sustained Drug Release and Photothermal Antibacterial Activity to Promote Full-Thickness Skin Regeneration During Wound Healing. *Small* 2019, *15* (12), 1900046.

(68) Liu, Y.; Niu, H.; Wang, C.; Yang, X.; Li, W.; Zhang, Y.; Ma, X.; Xu, Y.; Zheng, P.; Wang, J.; Dai, K. Bio-Inspired, Bio-Degradable Adenosine 5'-Diphosphate-Modified

Hyaluronic Acid Coordinated Hydrophobic Undecanal-Modified Chitosan for Hemostasis and Wound Healing. *Bioact. Mater.* **2022**, *17*, 162–177.

(69) Choi, J.; Reipa, V.; Hitchins, V. M.; Goering, P. L.; Malinauskas, R. A. Physicochemical Characterization and In Vitro Hemolysis Evaluation of Silver Nanoparticles. *Toxicol. Sci.* **2011**, *123* (1), 133–143.

(70) De Mel, A.; Chaloupka, K.; Malam, Y.; Darbyshire, A.; Cousins, B.; Seifalian, A. M. A Silver Nanocomposite Biomaterial for Blood-Contacting Implants. *J. Biomed. Mater. Res. Part A* **2012**, *100A* (9), 2348–2357.

(71) Laloy, J.; Minet, V.; Alpan, L.; Mullier, F.; Beken, S.; Toussaint, O.; Lucas, S.; Dogné, J. M. Impact of Silver Nanoparticles on Haemolysis, Platelet Function and Coagulation. *Nanobiomedicine* **2014**, *1*.

(72) Liu, Y.; Zhang, C.; Liu, L.; Zhang, X.; Hou, Y.; Zhao, L. Characterization of Chitin-Glucan Complex of Ganoderma Lucidum Extract and Its Application as Hemostatic Hydrogel. *Waste and Biomass Valorization* **2022**, *13* (7), 3297–3308.

(73) Putra, A.; Alif, I.; Hamra, N.; Santosa, O.; Kustiyah, A. R.; Muhar, A. M.; Lukman, K. MSC-Released TGF-β Regulate α-SMA Expression of Myofibroblast during Wound Healing.

J. Stem Cells Regen. Med. 2020, *16* (2), 73–79.

(74) Zhang, X.; Yin, M.; Zhang, L. J. Keratin 6, 16 and 17-Critical Barrier Alarmin Molecules in Skin Wounds and Psoriasis. *Cells* 2019, *8* (8).

(75) Ragothaman, M.; Palanisamy, T.; Kalirajan, C. Collagen-Poly(Dialdehyde) Guar Gum Based Porous 3D Scaffolds Immobilized with Growth Factor for Tissue Engineering Applications. *Carbohydr. Polym.* 2014, *114*, 399–406.

(76) Biscari, G.; Pitarresi, G.; Fiorica, C.; Schillaci, D.; Catania, V.; Palumbo, F. S.; Giammona, G. Near-Infrared Light-Responsive and Antibacterial Injectable Hydrogels with Antioxidant Activity Based on a Dopamine-Functionalized Gellan Gum for Wound Healing. *Int. J. Pharm.* 2022, *627*, 122257.

(77) Federico, S.; Catania, V.; Palumbo, F. S.; Fiorica, C.; Schillaci, D.; Pitarresi, G.; Giammona, G. Photothermal Nanofibrillar Membrane Based on Hyaluronic Acid and Graphene Oxide to Treat Staphylococcus Aureus and Pseudomonas Aeruginosa Infected Wounds. *Int. J. Biol. Macromol.* 2022, *214*, 470–479.

(78) Merlani, M.; Scheibel, D. M.; Barbakadze, V.; Gogilashvili, L.; Amiranashvili, L.; Geronikaki, A.; Catania, V.; Schillaci, D.; Gallo, G.; Gitsov, I. Enzymatic Synthesis and

Antimicrobial Activity of Oligomer Analogues of Medicinal Biopolymers from Comfrey and Other Species of the Boraginaceae Family. *Pharmaceutics* **2022**, *14* (1).

(79) Lenzuni, M.; Bonfadini, S.; Criante, L.; Zorzi, F.; Summa, M.; Bertorelli, R.; Suarato, G.; Athanassiou, A. Dynamic Investigation of Zein-Based Degradable and Hemocompatible Coatings for Drug-Eluting Stents: A Microfluidic Approach. *Lab Chip* **2023**, *23* (6), 1576–1592.

For Table of Contents Only